Korean J. Chem. Eng., **31**(11), 1954-1963 (2014)
DOI: 10.1007/s11814-014-0092-5

pISSN: 0256-1115
eISSN: 1975-7220

Low Reynolds number flow of power-law fluids over two square cylinders in tandem

Radhe Shyam and Rajendra Prasad Chhabra†

Department of Chemical Engineering, Indian Institute of Technology Kanpur, Kanpur 208016, India
(*Received 15 May 2013 • accepted 27 March 2014*)

Abstract−The governing partial differential equations have been solved numerically for the 2-D and steady power-law fluid flow over two square cylinders in tandem arrangement. Extensive numerical results spanning wide ranges of the governing parameters as Reynolds number ($0.1 \le Re \le 40$), power-law index ($0.2 \le n \le 1$) and inter-cylinder spacing ($2 \le L/d \le 6$) are presented herein; limited results for $L/d=24$ are also obtained to approach the single cylinder behavior. The detailed flow visualization is done by means of the streamline and vorticity contours in the vicinity of two cylinders. The global characteristics are analyzed in terms of the surface pressure distribution and pressure drag coefficient. The drag coefficient shows the classical inverse dependence on the Reynolds number irrespective of the value of the power-law index; the drag on the upstream cylinder is always greater than that for the downstream cylinder.

Keywords: Tandem Square Cylinders, Power-law Fluids, Reynolds Number, Drag Coefficient, Recirculation Length

INTRODUCTION

Owing to the wide occurrence of non-Newtonian fluid characteristics in scores of industrial settings including polymer, food, mineral, pharmaceutical and other processing applications, considerable research effort has been devoted to develop adequate understanding of transport processes in such fluids over the past 50-60 years. Consequently, a reasonably coherent body of knowledge has accrued as far as the flow of such fluids in pipes and ducts, mixing vessels, porous media, etc. is concerned [1-3]. On the other hand, the analogous body of information pertaining to the external flows is indeed not only very limited, but is also of recent vintage [2,4]. The bulk of the available studies relate to the flow past a sphere [2], a circular cylinder [4] and that over a single square cylinder [4]. Notwithstanding the fundamental significance of bluff-body fluid dynamics, the flow past cylinders of different cross-sections also denotes an idealization of numerous industrially important applications. Typical examples include the flow in tubular and pin-type heat exchangers, thermal treatment of foodstuffs, novel impeller designs to enhance the efficiency of mixing, measuring probes, cooling of electronic components and membrane-based separation modules, etc. [4]. Additional examples are found in the use of variously shaped objects to control the nature of flow by placing them at the entry of channels [5] and in compact heat exchangers [6,7]. Such model studies have proved to be of value in furthering our understanding of the underlying processes, but it is readily acknowledged that most practical situations entail multiple-cylinders arranged in different geometrical configurations, thereby leading to hydrodynamic interactions between adjacent cylinders [8,9]. The simplest configuration to understand such hydrodynamic interactions in multiple body situations is that of two-cylinders. Such configurations have been shown to serve as a useful starting point to understand inter-particle interactions in multiple-bluff body systems, e.g., see the works of Juncu [10] and Patil et al. [11] for two circular cylinders in Newtonian and power-law fluids, respectively. This study is thus concerned with the steady flow of power-law fluids over two-square cylinders in tandem arrangement, especially at low Reynolds numbers. It is instructive to recount the salient features of the currently available literature pertaining to the single and two square cylinders to facilitate the presentation of the present results.

Most industrial fluids of multiphase (suspensions, foams, emulsions, etc.) and polymeric (melts and solutions) nature exhibit a range of non-Newtonian characteristics, including shear-dependent viscosity (shear-thinning and shear-thickening), yield stress, and viscoelasticity [1-3]. However, most such systems display shear-thinning viscosity which decreases with the increasing shear rate under appropriate circumstances. It is thus reasonable to begin the analysis with the flow behavior of shear-thinning fluids, modeled here by the usual power-law model and the level of complexity can gradually be built up by incorporating the other non-Newtonian characteristics. Earlier studies in this field [12-15] were based on the assumption of the flow being steady up to about critical Reynolds number, $Re_{cr} \sim 45$, whereas the corresponding results in the vortex shedding regime were reported by Sahu et al. [16,17]. However, the limits of the flow detachment and that of the steady flow regime for an unconfined square cylinder in power-law fluids have been delineated only recently [18], which are lower than that for a circular cylinder. For the sake of completeness, the analogous body of knowledge pertaining to the flow of power-law fluids in the steady and in the laminar vortex shedding regimes past a single circular, semi-circular, triangular and elliptical cylinders has been reviewed elsewhere [4,19-23]. Therefore, in summary, reliable results of the momentum and heat transfer characteristics for square and circular cylinders in power-law fluids are available in the steady and laminar vortex shedding regime in confined and unconfined configurations. On the other hand, the analogous information for elliptical, triangular and semi-circular and circular cylinders is limited mainly to the steady flow regime [24-30].

†To whom correspondence should be addressed.
E-mail: chhabra@iitk.ac.in, rpc1953@yahoo.com

In contrast, the corresponding literature on two-square cylinders in a tandem arrangement is limited even in Newtonian fluids, let alone in power-law fluids. Most of the available experimental studies relate to wind tunnel conditions in which the Reynolds numbers tend to be of the order of 10^3-10^4, e.g., see [31-34]. The major thrust of these studies has been to elucidate the role of free stream turbulence intensity (0.2-4%) on the hydrodynamic forces and Strouhal number as a function of the varying inter-cylinder spacing (from the extreme case of L/d=0 equivalent to single cylinder to large inter-cylinder distance L/d=9). Indeed, depending upon the value of the inter-cylinder spacing and of the Reynolds number, a range of characteristics like hysteresis in drag [34], oscillating behavior [35], etc. have been observed both experimentally and numerically at such high Reynolds number. On the other hand, the numerical studies in this field have also focused on moderate Reynolds numbers in order to capture some of these trends [36,37]. To the best of our knowledge, only two numerical studies have focused on the flow over two square cylinders in the steady flow regime observed at low Reynolds numbers which are of interest here. For instance, Sohankar and Etminan [38] did a numerical study to determine the flow behavior (both steady and unsteady) over two square cylinders in tandem arrangement over the range of conditions $1 \le Re \le 200$, L/d=6. Similarly, for a fixed value of the center-to-center spacing of L/d=5, Chatterjee and Biswas [39] investigated the momentum and heat transfer characteristics across two square cylinders over the Reynolds number range $1 \le Re \le 30$ for three values of blockage ratios (defined as the side of the cylinder divided by the lateral height of the channel) as 0.05, 0.25 and 0.5 in order to delineate the influence of planar confinement. Over these ranges of conditions, the flow was found to be steady and the total drag coefficient decreased with the decreasing blockage. In a very recent study [40], the effect of power-law rheology on convective heat transfer has been reported for two square cylinders in tandem arrangement and the corresponding momentum transfer characteristics are reported herein. Very recently, two more studies appeared in the literature on this subject. Ehsan et al. [41] studied the flow of power-law fluids past two square cylinders in tandem arrangement to consider the influence of the power-law index, Reynolds number and inter-cylinder separation on the flow characteristics. While the range of the Reynolds number in their study is such that it spans both the steady and laminar vortex-shedding regimes, the bulk of their results pertain to the inter-cylinder gap of 6 and the Reynolds number value of 100, which is way beyond the steady flow regime. Similarly, Nifkarjam and Sohankar [42] also considered the momentum and heat transfer characteristics of this configuration in mildly non-Newtonian power-law fluids for a fixed value of the inter-cylinder gap of 5 for a fixed value of the Prandtl number of 0.71 (corresponding to air). While their drag values are in-line with the scant literature values, such a low value of the Prandtl number is rather unrealistic in the context of power-law fluids [1-3], thereby severely limiting the utility of their heat transfer results. In summary, with the exception of Shyam and Chhabra [40] and scant results reported in [41,42], no prior results are available on the flow of power-law fluids past a system of two square cylinders arranged in a tandem configuration, especially at low Reynolds numbers; The analogous configurations, however, involving two circular and two elliptic cylinders immersed in Newtonian and power-law fluids have been investigated in a few recent studies [10, 11,27-29]. Note also that not only such model configurations merit to be studied systematically to advance theoretical understanding of the underlying flow-phenomena, but these are also relevant in the context of the range of flow regimes observed in the channel flow fitted with a plane obstruction (like a plate), as reported by Kabir et al. [43]. The present work is thus concerned with the steady flow of power-law fluids over two square cylinders arranged in tandem configuration in the steady flow regime, thereby complementing the two recent studies in the laminar vortex shedding regime [41,42].

MATHEMATICAL FORMULATION

Consider the incompressible and steady flow of a power-law fluid, with a uniform velocity U_0 over two square cylinders (side d) in a tandem arrangement with center-to-center spacing of L in an unconfined space (Fig. 1(a)). Since it is impossible to simulate a truly unconfined flow, the two-cylinder system is enclosed here in an artificial cylindrical domain of diameter D with its center coincident with the mid-point between the two cylinders. Obviously, the selection of an optimum value of D is crucial to keep the computational effort at a reasonable level without a significant loss in accuracy of results. Over the range of Reynolds numbers of interest here, the flow is expected to be symmetric about the *x*-axis; therefore, the computations are performed only over half domain, i.e., $y \ge 0$, as shown in Fig. 1(b). Since both cylinders are infinitely long in the *z*-direction, the corresponding component of velocity U_z is assumed to be identically zero and there are no gradients in the *z*-direction. Under these conditions, the two-dimensional velocity and pressure fields are governed by the continuity and momentum balance equations written in their dimensionless form as follows:

$$\text{Continuity equation: } \nabla \cdot U = 0 \tag{1}$$

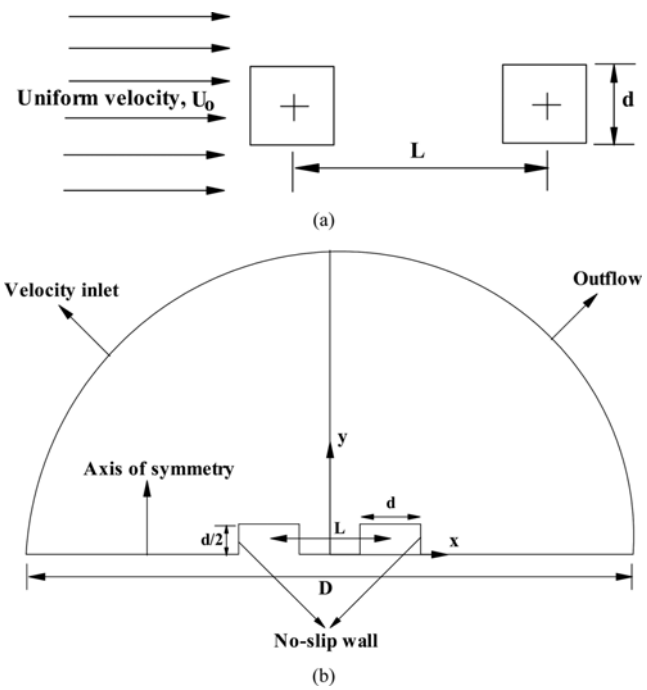

Fig. 1. (a) Schematic of the flow geometry, (b) Computational domain.

Momentum equation: $(U\cdot\nabla)\,U=-\nabla p+(1/Re)\,\nabla\cdot\sigma$ (2)

For an incompressible fluid, the components of the extra stress tensor (σ_{ij}) and rate of deformation tensor (ε_{ij}) are related as, $\sigma_{ij}=2\eta\varepsilon_{ij}$. The generalized viscosity function, η, for a power-law fluid is given by the expression, $\eta=(I_2/2)^{(n-1)/2}$ (see [1]). Here, n is the power-law index, which denotes the standard Newtonian behavior for n=1, whereas n<1 corresponds to shear-thinning behavior; I_2 is the second invariant of the rate of deformation tensor, which is given as follows: $I_2=\sum_i\sum_j \varepsilon_{ij}\varepsilon_{ji}$. Finally, it is necessary to specify the physically realistic boundary conditions for this flow configuration to complete the problem statement. The front half of the enclosing cylindrical envelope is designated as the inlet. At this surface, $U_x=1$; $U_y=0$ are used (Fig. 1(b)). At the surface of the two cylinders, the usual no-slip condition is used. Over the range of Reynolds numbers spanned here, the flow is expected to be steady and symmetric about the *x*-axis. The symmetry conditions have been employed at y=0 plane, $\partial U_x/\partial y=0$; $U_y=0$. The rear-half of the enclosing cylinder envelope is designated as the exit and it is reasonable to postulate that the disturbance introduced by the two cylinders would have subsided. In other words, it is equivalent to the assumption of fully developed flow at the exit boundary with no gradients in the *x*-direction, though the gradients can still exist in the lateral direction. This is similar to the Neumann type boundary condition.

The variables appearing in the foregoing differential equations and boundary conditions have been rendered dimensionless using d and U_0 as the linear and velocity scales, respectively. Thus, pressure is scaled by ρU_0^2; extra stress tensor components using $m(U_0/d)^n$; viscosity with $m(U_0/d)^{n-1}$, etc. The sole dimensionless parameter, namely, Reynolds number (Re), appearing in Eq. (2) is defined as: $Re=\rho d^n U_0^{2-n}/m$. Evidently, this flow is governed by three dimensionless groups: Reynolds number (Re), power-law index (n) and center-to-center separation (L/d). This work endeavors to elucidate the influence of each of these parameters on the momentum transfer characteristics for this flow configuration.

The aforementioned governing equations together with the specified boundary conditions have been solved numerically, thereby mapping the flow domain in terms of the primitive variables U_x, U_y and p. These, in turn, can be post processed to infer the values of the desired momentum parameters. It is customary to visualize the flow in terms of streamline and iso-vorticity contours in the close proximity of each cylinder and pressure distribution over these surfaces. At the next level, one can examine the behavior of the hydrodynamic drag force experienced by each cylinder, which describes the system hydrodynamics in an average sense. The recirculating wake region is characterized in terms of the recirculation length. It is thus appropriate to define some of these parameters here.

1. Recirculation Length

The recirculation length, L_r, is the distance between the rear stagnation point and the reattachment point of the nearby closed streamline at y=0 line. Thus, it is a measure of the length of the wake region in the axial direction.

2. Surface Pressure

The pressure coefficient, C_p, is a dimensionless form of the pressure on the surface of the cylinder given as: $C_p=2(P-P_0)/\rho U_0^2$, where, P is the local pressure at a point on the surface of each cylinder and P_0 is its reference value far away from the cylinders.

3. Drag Coefficient

Due to the prevailing shearing and normal stresses, there is a net force acting on each cylinder in the direction of flow. This is generally expressed using drag coefficient C_d which is made up of two components, namely, friction drag coefficient, C_{df} (due to shearing) and pressure drag coefficient, C_{dp} (due to normal stresses) defined as follows:

$$C_{df}=\frac{2F_{df}}{\rho U_0^2 d}=\frac{2^{n+1}}{Re}\int_S(\tau\cdot n_s)dS \tag{3}$$

$$C_{dp}=\frac{2F_{dp}}{\rho U_0^2 d}=\int_S C_p n_x dS \tag{4}$$

Thus, the fluid mechanical aspects of the problem studied here are analyzed in terms of the streamline and vorticity contours in close proximity of the two cylinders, whereas the overall characteristics are captured in terms of the drag coefficients as functions of Reynolds number, power-law index and center-to-center gap between the two cylinders. Owing to the steady and symmetric nature of the flow, no lift force is expected over the range of conditions spanned here.

NUMERICAL SOLUTION METHODOLOGY AND CHOICE OF NUMERICAL PARAMETERS

Since a detailed description of the numerical solution procedure used here is available elsewhere [40], it is not repeated here and only the salient features are given. The field equations together with the boundary conditions outlined in the preceding section have been solved numerically using the finite volume based solver ANSYS Fluent (version 6.3.26). The second-order upwind (SOU) scheme was used to discretize the convective terms in the momentum equations. The SIMPLE (semi-implicit method for the pressure linked equations) scheme was used to solve the momentum equations. A simulation was deemed to have converged when the residuals of the continuity, *x*-momentum and *y*-momentum equations had dropped below 10^{-8}. Within the framework of this criterion, the drag values had stabilized at least up to four significant digits. The constant density and non-Newtonian power-law models were used to input the physical properties of the fluid to achieve the desired values of the Reynolds number. However, these values are of no particular significance, because the present results are reported in terms of the relevant dimensionless parameters.

Since a detailed discussion regarding the choice of numerical parameters like optimum computational mesh, value of D and convergence criterion is available elsewhere [40], based on a similar extensive exploration, (D/d)=800 and (D/d)=400 were found to be adequate for Re<1 and Re≥1, respectively. Similarly, an inner region extending up to a radius of 4d to 6d depending upon the value of L/d (20d for L/d=24), is meshed using an unstructured grid; beyond this region, a structured grid with a stretching ratio <1.1 is used. Based on such tests, for Re<1, a grid characterized by δ/d=0.004, N_p=320, N_{cell}=153, 970 was found to be adequate in the present work. Similarly, for Re≥1, a grid characterized by δ/d=0.008, N_p=240, N_{cell}=137, 960 was found to be satisfactory. The adequacy of the domain and grid selected here is further demonstrated by presenting a few benchmark comparisons in the next section.

RESULTS AND DISCUSSION

1. Validation

To establish the reliability and accuracy of the numerical solution methodology used here, three benchmark problems have been studied. Reliable numerical results are now available for the laminar flow of Newtonian [44] and power-law fluids [45,46] in a lid-driven square cavity geometry. For a fixed value of Re=100 (based on the side length of the cavity) for various values of n=0.5, 0.75, 1 and 1.5, the present values of the *x*- and *y*-components of the velocity at the centerline of the cavity were found to be within ±1% of the literature values. Similarly, Fig. 2 shows a comparison between the present results and that of Sohankar and Etminan [38] in terms of the drag coefficient (C_d) and recirculation length (L_r) as functions of the Reynolds number for the two tandem square cylinders in Newtonian fluids with the center-to-center separation of L/d=6. Once again, the two results are seen to be in excellent agreement; the two drag values differ from each other by 3.6% and 4.5% for the upstream and downstream cylinders respectively, whereas the value of L_r differs by 9% at Re=5; the difference between the two values decreases

Table 1. Comparison of present results with the values of Chatterjee and Biswas [39]

Re	Present		Chatterjee and Biswas [39]	
	C_{dup}	C_{ddown}	C_{dup}	C_{ddown}
5	4.9881	2.3576	5.0145	2.4306
10	3.3995	1.4034	3.3954	1.4079
20	2.4274	0.8155	2.4182	0.8033
30	2.0374	0.5654	1.9876	0.5466

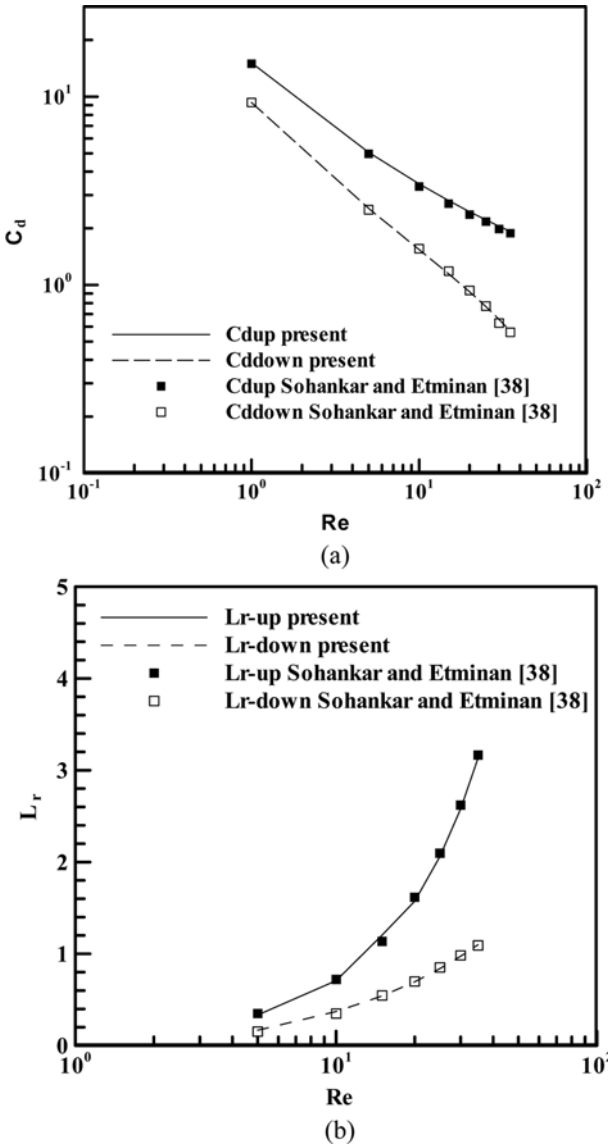

Fig. 2. Comparison of (a) Drag coefficient (C_d) and (b) Recirculation length (L_r) with Sohankar and Etminan [38] at L/d= 6, n=1.

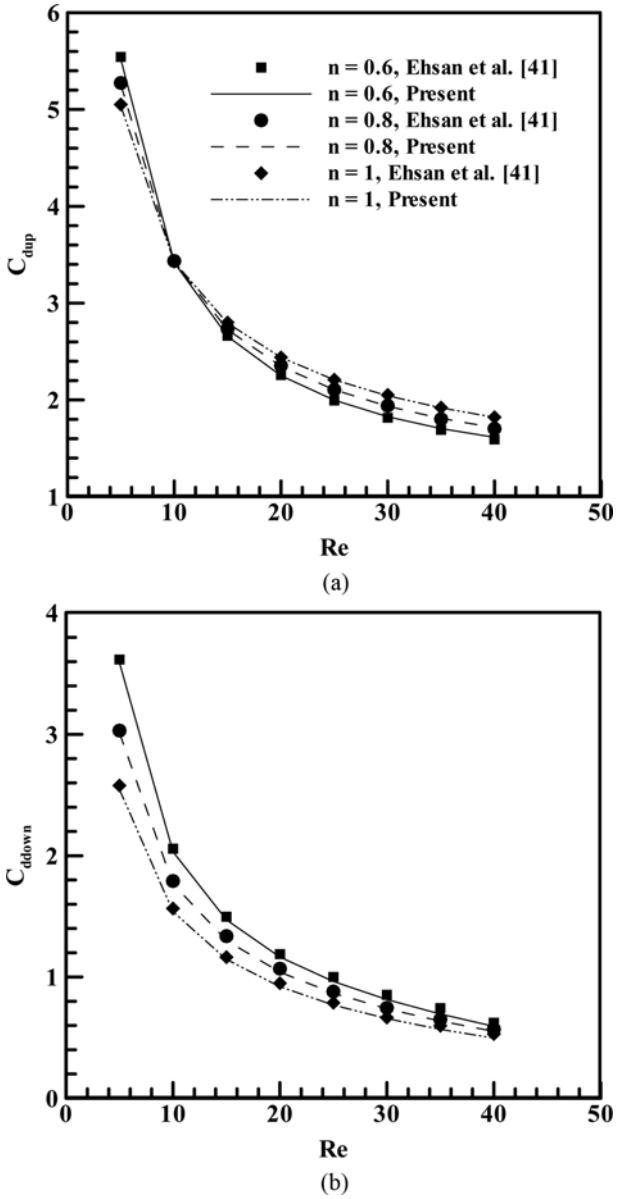

Fig. 3. (a) Comparison of present C_{dup} values (line) with data (symbols) of Ehsan et al. [41] for L/d=6. (b) Comparison of present C_{ddown} values (line) with data (symbols) of Ehsan et al. [41].

with the increasing value of the Reynolds number. This seemingly large discrepancy between the present results and that of Sohankar and Etminan [38] is presumably due to the fact that the recirculation length is very small at Re=5. Next, Chatterjee and Biswas [39] studied the effect of confinement for this configuration at low Reynolds numbers. Strictly speaking, the present results cannot be compared with their values, but Table 1 contrasts the two sets of results for the lowest value of the confinement (5%) when the influence of a confining wall is expected to be negligible. Bearing in mind the differences inherent in these two studies, the correspondence is seen to be very good. Similarly, Fig. 3 shows a comparison between the present results and that of Ehsan et al. [41] for L/d=6 and for three values of the power-law index; an excellent correspondence is seen to exist between the two predictions and the maximum discrepancy is of the order of 4.5%. Finally, the present values of the Nusselt number are within ±5% of that reported recently in the literature [42]. In addition to the above benchmark comparisons, the present results for the upstream cylinder at L/d=24 are also compared (Table 2) with the single cylinder results of Rao et al. [18]. The two drag values are seen to differ at most by 3.4%, which is considered to be acceptable, thereby suggesting that the upstream cylinders behaves independently of the downstream one at such large values of (L/d). The foregoing discussion together with the additional validation reported in our previous paper [40] lends credibility to the reliability and accuracy of the present solution methodology and the choice of numerical parameters. The present new results for the two cylinders in tandem in power-law fluids are therefore considered to be reliable to within 2-3%.

Table 2. Comparison of present upstream cylinder (at L/d=24) drag coefficient (C_d) with single cylinder of Rao et al. [18]

	Re=5		Re=40	
	n=0.2	n=1	n=0.2	n=1
Present	6.58	4.31	1.45	1.64
Rao et al. [18]	6.61	4.46	1.49	1.67

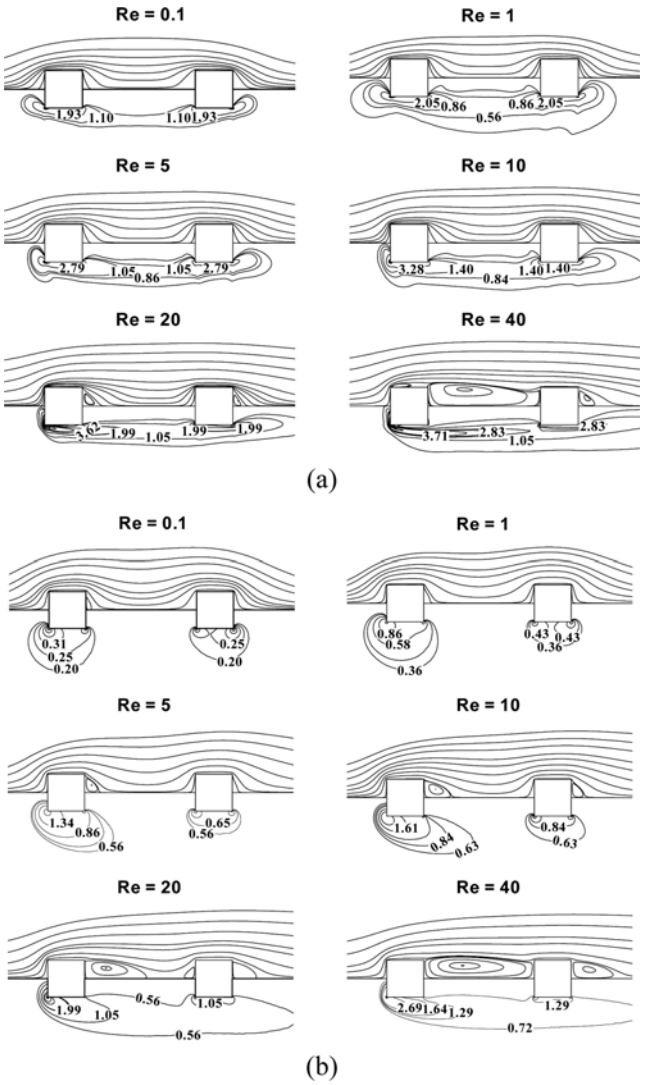

Fig. 4. Effect of Reynolds number on streamline (upper half) and vorticity (lower half) contour patterns at L/d=4, (a) n=0.2, (b) n=1.

2. Detailed Flow Characteristics

It is customary to visualize the structure of the flow field by means of streamline and vorticity contours in the proximity of the square cylinders as functions of the Reynolds number, power-law index and center-to-center spacing between the cylinders. Figs. 4-6 show representative streamline (upper half) and iso-vorticity contours (lower half) for the range of conditions spanned here. As expected, at low Reynolds numbers (Re≤≈1), the flow remains attached to the surface of the cylinder irrespective of the value of the power-law index or of the gap between the two-cylinders, except at the lowest value of L/d=2 used here. This observation is consistent with the fact that the flow separates from a single cylinder in Newtonian fluids at about Re~1.2-1.3 [18]. Similarly, the critical Reynolds number exhibits a non-monotonic dependence on power-law index (n), i.e., exhibiting its maximum value of ~3.2-3.3 in the vicinity of n~0.5 and then dropping to a value of ~1.2-1.3 again for a highly shear-thinning (n=0.2) fluid, which is also close to the critical Reynolds number in Newtonian fluids. Thus, the present results for the upstream cylinder are in line with the previous values reported in the literature. The downstream cylinder also exhibits qualitatively similar trends, especially at large values of L/d when the interactions between the cylinders are weak. Of course, for Re>5, there is a well-developed recirculating region behind each cylinder irrespective of the value of L/d and/or of the power-law index (n). The results shown in Figs. 4(a) and 4(b) at Re=40 are particularly striking as the downstream cylinder impedes the full development of the wake of the preceding cylinder in the both Newtonian and shear-thinning fluids, as the length of the wake for a single cylinder is expected to be of the order of ~3d [18], which is very close to the gap between the two cylinders. Fig. 5 shows the influence of power-law index on the flow patterns at Re=40. At Re=0.1, no flow separation is seen to occur. However, at Re=40, downstream cylinder causes disturbance in the flow field in between the two cylinders. Since the wake length grows with the decreasing degree of shear-thinning, interference is seen to be maximum in Newtonian fluids. This can be explained, at least qualitatively, by acknowledging that the effective viscosity of a shear-thinning fluid increases rapidly away from the regions of high deformation rates, thereby suppressing the size of the wake. Conversely, the momentum boundary layers are known to be thin-

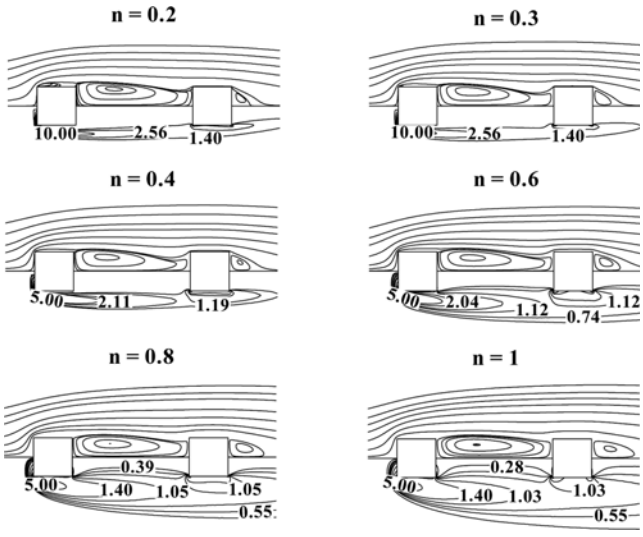

Fig. 5. Effect of power-law index on streamline (upper half) and vorticity (lower half) contour patterns at L/d=4, Re=40.

ner in power-law fluids otherwise under identical conditions [3]. Fig. 6 clearly shows the decreasing interference between the two cylinders with the increasing inter-cylinder separation. The wake of the trailing cylinder is seen to be shorter than that of the leading cylinder due to the distortion of the velocity profile of the oncoming stream impinging on the trailing cylinder. It is appropriate to mention here that while the streamline and iso-vorticity contours shown in the preceding figures are obviously based on the same numerical data, but since all contours cannot be included in all figures, and therefore, these might appear different in some cases. Also, the basic purpose of such plots is to display the general flow patterns.

It is also interesting that a common recirculation region is formed in between the two cylinders even at Re=0.1 and L/d=2. This is obviously due to flow separation in the rear of the leading cylinder and on the front of the trailing cylinder, as also reported by Tatsuno [47] for two circular cylinders in the Reynolds number range, Re< ~0.2 at about L/d=2 in Newtonian fluids, whereas no such separation was observed at L/d=3. On the other hand, they also reported the widening of this recirculation region in the lateral direction at L/d≈1.7, thereby suggesting squeezing of the fluid by the decreasing gap between the two cylinders. These results are also qualitatively consistent with the trends reported for two circular cylinders in power-law fluids [11]. Note that, for a single square cylinder, the flow remains attached to cylinder surface at such low values of the Reynolds number and, therefore, the behavior seen here can be safely ascribed to the strong interference effects at L/d=2. Similarly, with the increasing Reynolds number, the flow can separate at the leading corners, which may or may not reattach itself at the rear corners. When reattachment occurs, the two recirculating regions behave independently of each other, whereas the two are connected in the absence of flow reattachment. This behavior is also in line with the behavior seen for two circular cylinders [11]. This leads to further modifications in the flow field.

The lower-half of each figure shows the corresponding vorticity contours. As expected, the vorticity is seen to be maximum at the surface of the cylinder due to the imposition of the no-slip condi-

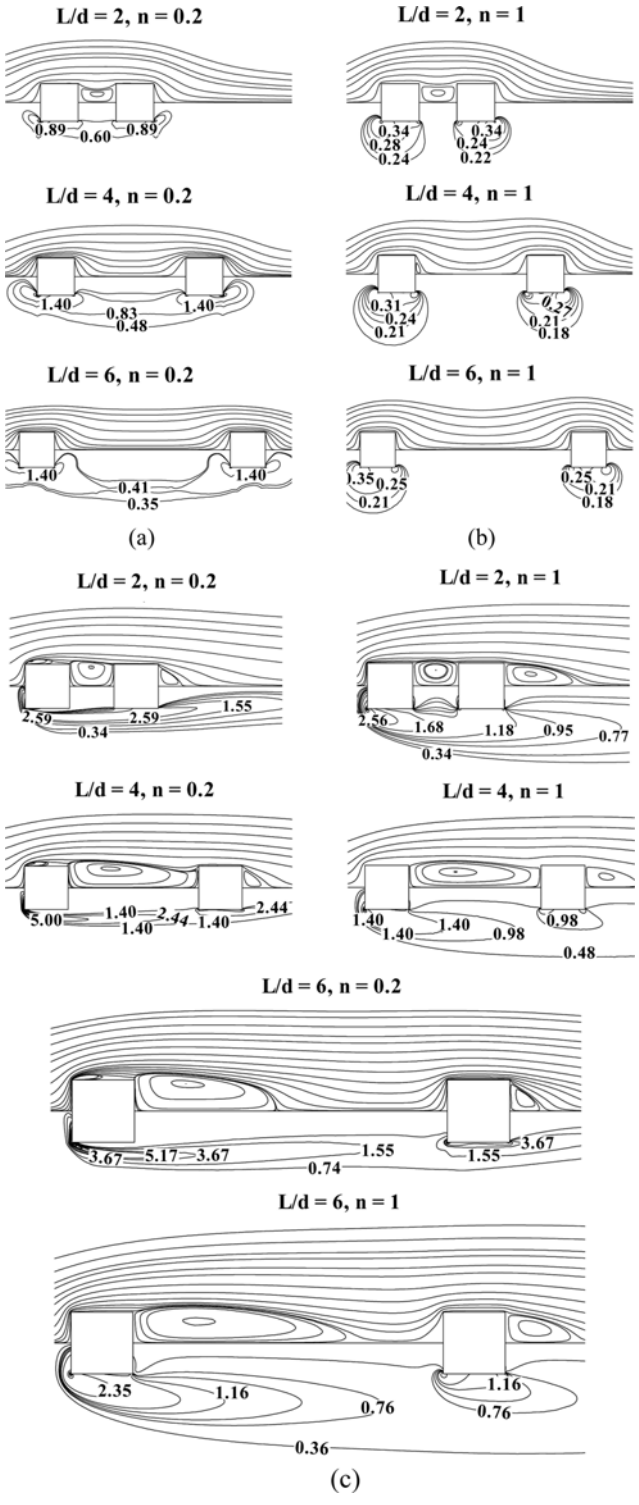

Fig. 6. Effect of L/d ratio on streamline (upper half) and vorticity (lower half) contour patterns. (a) Re=0.1, n=0.2, (b) Re= 0.1, n=1. (c) Re=40, n=0.2 and 1.

tion, and it progressively decreases away from each cylinder due to the diminishing velocity gradients. At low Reynolds numbers, the vorticity values are comparable for both cylinders, particularly in the absence of wake formation in the rear of the upstream cylinder. However, with the appearance of the recirculation zone, the vortic-

ity values are much smaller for the rear cylinder than that of the upstream cylinder due to the modifications of the velocity field incident on the downstream cylinder. Broadly, for fixed values of L/d and n, the vorticity level increases with the increasing Reynolds number. On the other hand, for a fixed value of the Reynolds number and L/d, the magnitude of vorticity increases with the increasing degree of shear-thinning. This is presumably so due to the thinning of the boundary layer, thereby increasing the velocity gradient. Finally, for fixed values of Re and n, vorticity shows very little influence of L/d at low Reynolds numbers. This is because the flow remains attached to the surface of each cylinder except for the severe interference effect seen at L/d=2. However, once the flow detaches from the surface of the cylinder, the vorticity values increase. In the latter case, the vorticity is seen to decrease spatially somewhat faster in shear-thinning fluids than that in Newtonian fluids.

Fig. 7 shows the functional dependence of the recirculation length on the Reynolds number (Re), power-law index (n) and inter-cylinder gap (L/d). At the lowest value of the inter-cylinder gap (L/d=2) as noted previously, there is a common recirculation region in between the two cylinders, and therefore, L_r cannot be defined for the upstream cylinder, albeit the results for the downstream cylinder are included here. Broadly, the recirculation length shows qualitatively similar dependence on the Reynolds number in both Newtonian and power-law liquids. However, the flow separation is somewhat delayed in shear-thinning fluids, and the recirculation length also tends to be shorter in shear-thinning fluids than that in Newtonian media otherwise under identical conditions. The results of Rao et al. [18] for a single square cylinder are also included in this figure. It is noted that the recirculation length of the upstream cylinder at L/d=6 is close to the single cylinder value, which also signifies the fact that tandem cylinder results approach the single cylinder behavior at large L/d ratios.

3. Surface Pressure Distribution

At the next level, one can gain further insights by examining the

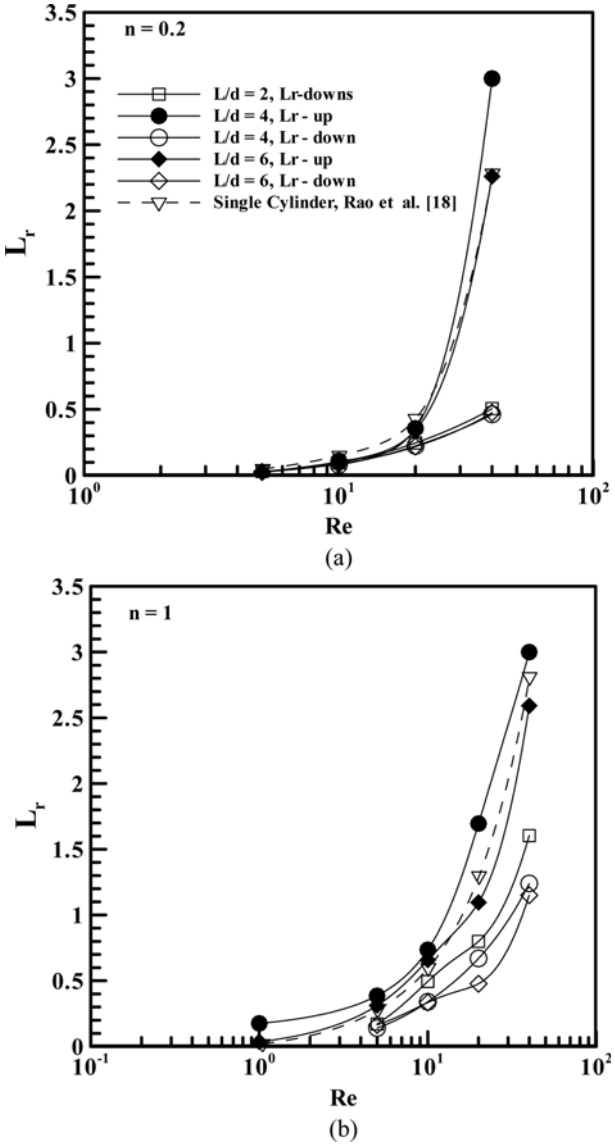

Fig. 7. Effect of Reynolds number on recirculation length (a) n= 0.2 (b) n=1.

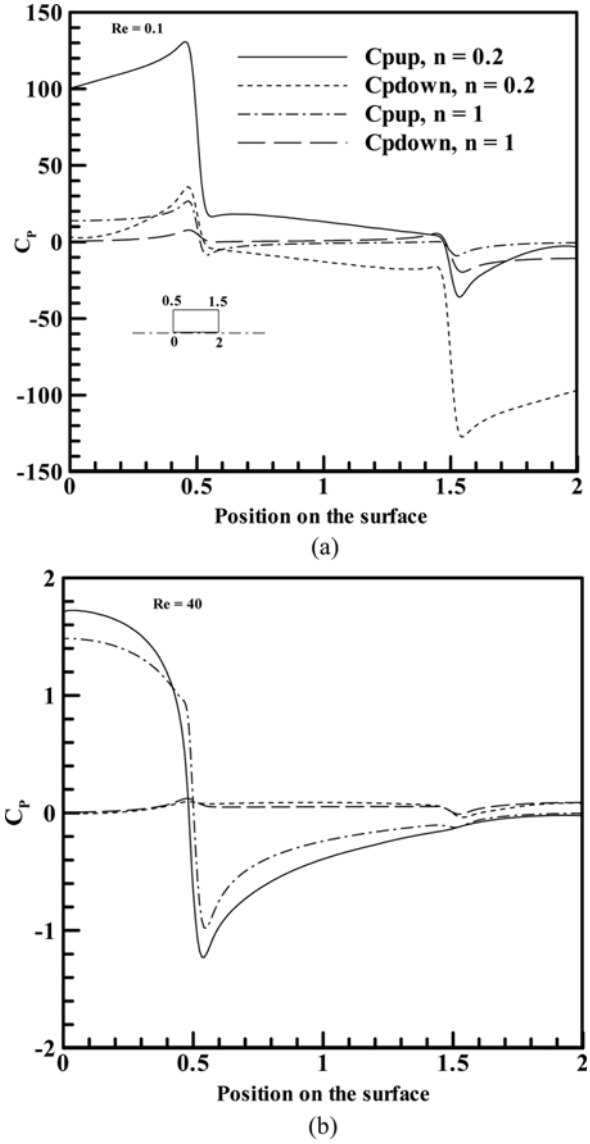

Fig. 8. Typical variation of surface pressure, C_p, on half of cylinder surface at L/d=2 (a) Re=0.1 (b) Re=40.

surface pressure profiles on the surface of each cylinder. Fig. 8 shows representative surface pressure results for n=0.2 and 1 and Re=0.1 and 40 at L/d=2. At low Reynolds numbers, for the upstream cylinder, the surface pressure gradually increases from the front stagnation point towards the corner and then it rapidly decreases and remains nearly constant up to the rear corner, reaching its minimum value just after the corner followed by a slight recovery. The corresponding results for the trailing cylinder show qualitatively similar trends except for the fact that surface pressure values at congruous points are much lower, akin to as if the trailing cylinder is submerged in the low pressure wake region formed in the gap in between the two cylinders, showing the minimum pressure at the rear corner. On the other hand, the effect of power-law index is seen to be much more dramatic on the upstream cylinder in the front half, whereas it manifests in the rear of the trailing downstream cylinder. The effect of power-law index is seen to progressively diminish with the increasing Reynolds number, e.g., see Fig. 8(b) at Re= 40. This is not at all surprising because the role of viscous forces diminishes with the increasing Reynolds number, and hence the value of power-law index is of little relevance under these conditions. Also, due to the separation in the rear of the upstream cylinder, there is very little variation in the surface pressure of the trailing cylinder, and over most of the surface of the trailing cylinder, the pressure is negative.

4. Drag Coefficient

Evidently, both the total (C_d) and pressure (C_{dp}) drag coefficients are expected to be functions of Re, (L/d) and n, as shown in Figs. 9 and 10. For fixed values of power-law index (n) and (L/d), both the overall and pressure (not shown in Fig. 10 in the interest of clarity) drag coefficients exhibit the classical inverse dependence on the Reynolds number. Furthermore, the drag value of the upstream cylinder is influenced very little by the value of (L/d), and indeed this effect progressively diminishes with the increasing values of (L/d) or Reynolds number or both. On the other hand, this effect is seen to be fairly strong at low Reynolds numbers due to the merging of the recirculation region formed in the rear of the upstream cylinder with that in front of the downstream cylinder. Further detailed examination of the results revealed that shear-thinning behavior enhances drag at low Reynolds numbers over and above that seen in Newtonian fluids. This is obviously due to the dominance of viscous forces at such Reynolds numbers. For instance, at Re=0.1, the total drag and its pressure component of the both upstream and downstream cylinders can be about ~5 times higher in a highly shear-thinning fluid (n=0.2) than that in a Newtonian fluid (n=1). On the other hand, at Re=40, both components vary by less than 5-10% as the value of the power-law index, n, is gradually decreased from n=1 to n=0.2. Under these conditions, the flow is dominated by the inertial forces and hence the viscous characteristics are of little relevance. Furthermore, at such high Reynolds numbers, the ratio of pressure and friction drag contributions remains more or less constant for the downstream cylinder, whereas it gradually increases with the

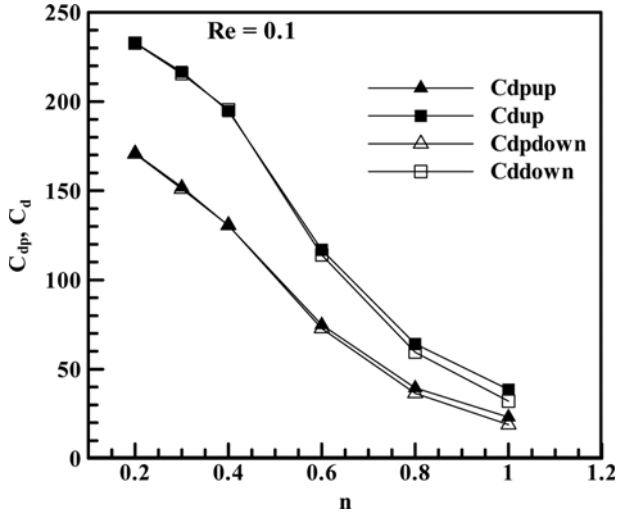

Fig. 9. Effect of power-law index on pressure drag coefficient (C_{dp}) and total drag coefficient (C_d) of upstream and downstream cylinders at L/d=4, Re=0.1.

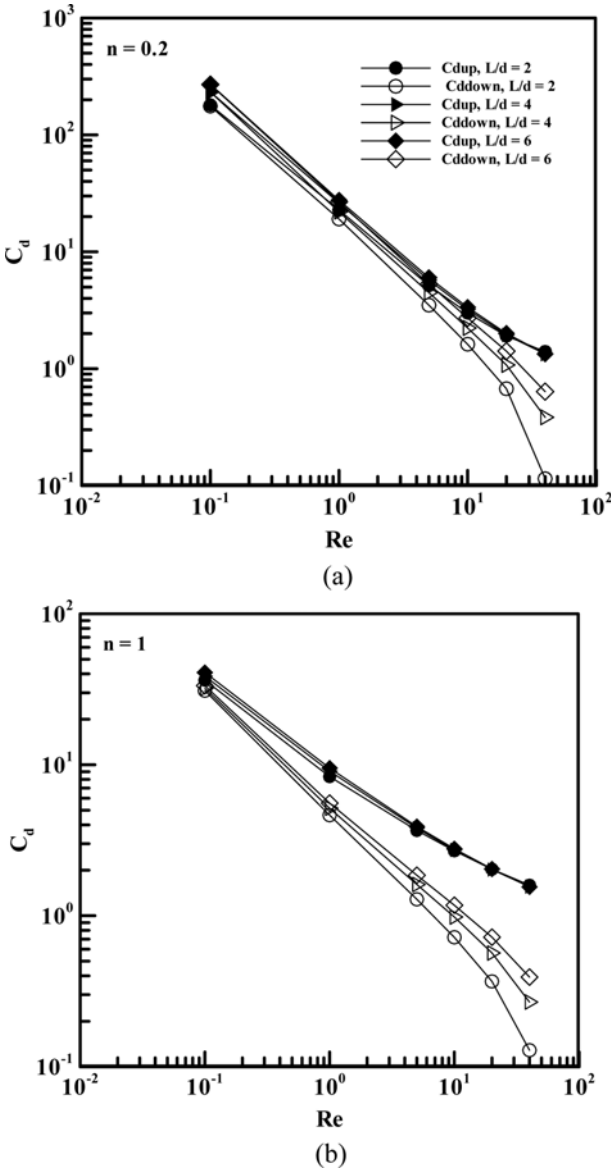

Fig. 10. Effect of Reynolds number and inter-cylinder spacing on the total drag coefficients of upstream and downstream cylinders, (a) n=0.2 (b) n=1.

increasing Reynolds number in both Newtonian and shear-thinning fluids for the upstream cylinder. These trends are also consistent with the surface pressure profiles seen in the preceding section.

CONCLUSIONS

The effect of power-law fluid rheology on the momentum transfer characteristics for two square cylinders in tandem arrangement has been studied over the range of Reynolds number ($0.1 \le Re \le 40$) such that the flow regime is steady and two-dimensional. Qualitatively, the overall characteristics seen here tend to be similar to that observed for two circular cylinders. For instance, when the two cylinders are placed very close to each other, even at low Reynolds numbers, the flow separates from the rear corner of the upstream cylinder and from the front corner of the trailing cylinder, and these two separated flow regions merge into one. On the other hand, in highly shear-thinning fluids, the flow also separates from the front corner at lower values of Reynolds numbers than that in Newtonian fluids. Broadly, at fixed values of the Reynolds number, recirculation regions tend to be somewhat shorter in shear-thinning fluids than that in Newtonian fluids and, therefore, this leads to weaker interference induced by the trailing cylinder. While at low Reynolds numbers, shear-thinning behavior enhances the drag on each cylinder over and above their values in Newtonian fluids otherwise under identical conditions; this effect diminishes rapidly with the increasing Reynolds number. Finally, the relative contribution of the pressure component to the overall drag is modulated both by the values of the Reynolds number and power-law index, especially for the trailing cylinder.

NOMENCLATURE

C_d : drag coefficient, dimensionless
C_{df} : friction drag coefficient, dimensionless
C_{dp} : pressure drag coefficient, dimensionless
C_p : pressure coefficient, dimensionless
d : side of cylinder [m]
D : diameter of computational domain [m]
F_{df} : friction drag force per unit length of cylinder [N/m]
F_{dp} : pressure drag force per unit length of cylinder [N/m]
I_2 : second invariant of rate of deformation tensor, dimensionless
L : centre-to-centre spacing between the two cylinders [m]
L_r : recirculation length, dimensionless
m : power-law consistency index [$Pa \cdot s^n$]
N_{cell} : total number of cells in the computational domain (half), dimensionless
N_p : number of grid points on half of the cylinder circumference, dimensionless
n : power-law index, dimensionless
n_s : unit vector normal to the surface, dimensionless
n_x : unit normal vector along the x-direction, dimensionless
p : pressure, dimensionless
P : pressure [Pa]
Re : Reynolds number, dimensionless
S : surface area of each cylinder [m^2]
U : velocity vector, dimensionless
U_0 : free stream velocity [m/s]

Greek Symbols

δ : smallest cell size on the cylinder surface [m]
ρ : fluid density [kg/m^3]
σ_{ij} : extra stress tensor, dimensionless
ε_{ij} : rate of deformation tensor, dimensionless
η : apparent viscosity, dimensionless

Subscripts

i, x : x-component
j, y : y-component
up : upstream cylinder
down : downstream cylinder

REFERENCES

1. R. B. Bird, R. C. Armstrong and O. Hassager, *Dynamics of polymeric liquids, Vol. 1: Fluid Dynamics*, 2nd Ed., Wiley, New York (1987).
2. R. P. Chhabra, *Bubbles, drops and particles in non-newtonian fluids*, 2nd Ed., CRC Press, Boca Raton, FL (2006).
3. R. P. Chhabra and J. F. Richardson, *Non-newtonian flow and applied rheology*, 2nd Ed., Butterworth-Heinemann, Oxford (2008).
4. R. P. Chhabra, *Advances in Heat Transfer*, **43**, 289 (2011).
5. M. A. Kabir, M. M. K. Khan and M. G. Rasul, *Chem. Eng. Commun*, **199**, 689 (2012).
6. J. E. Hesselgreaves, *Compact heat exchangers*, Pergamon Press, Oxford (2001).
7. S. Kakac and H. Liu, *Heat exchangers: Selection, rating and thermal design*, 2nd Ed., CRC Press, Boca Raton, FL (2002).
8. M. M. Zdravkovich, *Flow around circular cylinders, Vol. 1: Fundamentals*, Oxford University Press, New York (1997).
9. M. M. Zdravkovich, *Flow around circular cylinders, Vol 2: Applications*, Oxford University Press, New York (2003).
10. G. Juncu, *Int. J. Heat Mass Transfer*, **50**, 3788 (2007).
11. R. C. Patil, R. P. Bharti and R. P. Chhabra, *Ind. Eng. Chem. Res.*, **47**, 1660 (2008).
12. A. K. Dhiman, R. P. Chhabra and V. Eswaran, *Chem. Eng. Res. Des.*, **84**, 300 (2006).
13. A. K. Dhiman, R. P. Chhabra and V. Eswaran, *J. Non-Newtonian Fluid Mech*., **148**, 141 (2008).
14. A. K. Dhiman, *Int. J. Therm. Sci*., **48**, 1552 (2009).
15. M. Bouaziz, S. Kessentini and S. Turki, *Int. J. Heat Mass Transfer*, **53**, 5420 (2010).
16. A. K. Sahu, R. P. Chhabra and V. Eswaran, *J. Non-Newtonian Fluid Mech.*, **160**, 157 (2009).
17. A. K. Sahu, R. P. Chhabra and V. Eswaran, *J. Non-Newtonian Fluid Mech*., **165**, 752 (2010).
18. P. K. Rao, A. K. Sahu and R. P. Chhabra, *Int. J. Heat Mass Transfer*, **54**, 390 (2011).
19. V. K. Patnana, R. P. Bharti and R. P. Chhabra, *Chem. Eng. Sci.*, **64**, 2978 (2009).
20. V. K. Patnana, R. P. Bharti and R. P. Chhabra, *Int. J. Heat Mass Transfer*, **53**, 4152 (2010).
21. A. Dhiman and R. Shyam, *ISRN Mech. Eng.*, **2011**, 1 (2011).
22. M. K. Rao, A. K. Sahu and R. P. Chhabra, *Polym. Eng. Sci*., **51**, 2044

(2011).
23. S. Bijjam and A. K. Dhiman, *Chem. Eng. Commun*., **199**, 767 (2012).
24. P. K. Rao, A. K. Sahu and R. P. Chhabra, *Ind. Eng. Chem. Res*., **49**, 6649 (2010).
25. A. Prhashanna, A. K. Sahu and R. P. Chhabra, *Int. J. Therm. Sci*., **50**, 2027 (2011).
26. A. Chandra and R. P. Chhabra, *Int. J. Heat Mass Transfer*, **54**, 2734 (2011).
27. N. S. K. Chaitnya and A. K. Dhiman, *Int. J. Heat Mass Transfer*, **55**, 5941 (2012).
28. A. Nejat, V. Abdollahi and K. Vahidkhah, *J. Non-Newtonian Fluid Mech*., **166**, 689 (2011).
29. E. Nejat, E. Mirzakhalili, A. Aliakbari, M. S. F. Niasar and K. Vahidkhah, *J. Non-Newtonian Fluid Mech.*, **171-172**, 67 (2012).
30. A. K. Dhiman and S. Kumar, *Korean J. Chem. Eng.*, **30**, 33 (2013).
31. H. Sakamoto and H. Haniu, *J. Wind Eng. Ind. Aerod*., **31**, 41 (1988).
32. H. Suzuki, Y. Inoue, T. Nishimura, K. Fukutani and K. Suzuki, *Int. J. Heat Fluid Flow*, **14**, 2 (1993).
33. S. C. Luo, L. L. Li and D. A. Shah, *J. Wind Eng. Ind. Aerod*., **79**, 79 (1999).
34. C. H. Liu and J. M. Chen, *J. Wind Eng. Ind. Aerod*., **90**, 1019 (2002).
35. A. Valencia, *Heat Mass Transfer*, **33**, 465 (1998).
36. A. Lankadasu and S. Vengadesan, *Int. J. Numer. Methods Fluids*, **57**, 1005 (2008).
37. J. L. Rosales, A. Ortega and J. A. C. Humphrey, *Int. J. Heat Mass Transfer*, **44**, 587 (2001).
38. A. Sohankar and A. Etminan, *Int. J. Numer. Methods Fluids*, **60**, 733 (2009).
39. D. Chatterjee and G. Biswas, *Numer. Heat Transfer A*, **59**, 437 (2011).
40. R. Shyam and R. P. Chhabra, *Int. J. Heat Mass Transfer*, **57**, 742 (2012).
41. I. Ehsan, S. Mohammad, N. M. Reza, J. Ali and E. S. Tashnizi, *J. Fluids Engineering (ASME)*, **135**, 061101-1 (2013).
42. F. Nikfarjam and A. Sohankar, *Acta Mech*., **224**, 1115 (2013).
43. M. A. Kabir, M. M. K. Khan and M. A. Bhuiyan, *KSME International J.*, **17**, 879 (2003).
44. U. Ghia, K. N. Ghia and C. T. Shin, *J. Comput. Phys*., **48**, 387 (1982).
45. B. C. Bell and K. S. Surana, *Int. J. Numer. Methods Fluids*, **18**, 127 (1994).
46. P. Neofytou, *Adv. Eng. Soft*., **36**, 664 (2005).
47. M. Tatsuno, *Fluid Dyn. Res*., **5**, 49 (1989).